Available online at www.sciencedirect.com
ScienceDirect
Synthetic Metals 156 (2006) 1139–1147
SYNTHETIC METALS
www.elsevier.com/locate/synmet

Synthesis, characterization and low frequency AC conduction of polyaniline/niobium pentoxide composites☆

Y.T. Ravikiran[a], M.T. Lagare[a], M. Sairam[b], N.N. Mallikarjuna[c], B. Sreedhar[d], S. Manohar[c], A.G. MacDiarmid[c], T.M. Aminabhavi[b,*]

[a] *Department of Physics, Gulbarga University, Gulbarga 585106, India*
[b] *Center of Excellence in Polymer Science, Karnatak University, Dharwad 580003, India*
[c] *Alan G. MacDiarmid Laboratory for Innovative Research, The University of Texas at Dallas, Richardson, TX 75080, United States*
[d] *Inorganic and Physical Chemistry Division, Indian Institute of Chemical Technology, Hyderabad 500007, India*

Received 28 November 2005; received in revised form 19 July 2006; accepted 1 August 2006

Abstract

New types of conducting polyaniline–niobium pentoxide (PANI/Nb_2O_5) nanocomposites have been synthesized by in situ deposition technique by placing fine grade powder of Nb_2O_5 during in situ polymerization of aniline. The composites formed were characterized by X-ray diffraction (XRD), X-ray photoelectron spectroscopy (XPS), scanning electron microscopy (SEM), transmission electron microscopy (TEM) and thermogravimetric analysis (TGA). XRD and TEM indicated the dominant role-played by Nb_2O_5 particles, whereas XPS indicated incomplete protonation of imine moieties. SEM images indicated a systematic morphological variation of particles aggregated in the composite matrix as compared to the pristine PANI. Three step decomposition patterns were observed for PANI and its composites. AC conductivity and dielectric response of the composites were investigated in the frequency range, 10^2–10^6 Hz. AC conductivity obeyed the power law index, which decreased with increasing wt.% of Nb_2O_5. PANI showed high dielectric constant, which could be related to conductivity relaxation phenomenon. Both dielectric constant and dielectric loss decreased with increasing wt.% of Nb_2O_5. Variations in measured AC response parameters with increasing Nb_2O_5 contents of the composite followed systematic trends that are similar to those observed with decreasing temperature and level of doping.

Keywords: Polyaniline; Niobium pentoxide; Polymer composites; Electrical properties; Scanning electron microscopy; Thermogravimetric analysis

1. Introduction

Heterogeneous conducting polymer composites, especially organic–inorganic nanocomposites, have been the subject of extensive study in recent years [1–4]. Among the base materials used, polyaniline (PANI) is one of the most extensively studied conducting polymer, ever since its pioneering discovery by MacDiarmid et al. [5,6]. PANI has attracted considerable attention since then to prepare composites by incorporating inorganic particles like $BaTiO_3$ [7], molybdenum trisulfide [8], V_2O_5 [9], inorganic salts [10], montmorillonite [11], TiO_2 [12], ZrO_2 [13], etc. Polyaniline–inorganic particle composites have been studied for applications as electro-rheological fluids [14] and in high density information storage devices [15]. Successful preparation of magnet containing conducting polymer has been reported by Tang et al. [16,17]. However, the combination of conducting polymers with a host of foreign materials having different characteristics opens up novel avenues to develop hybrid materials showing interesting properties. Different conformations of polymeric chains in the interlayer spaces could enable to further characterize such polymers.

In the present research, preparation of conducting PANI composites with a transition metal oxide such as niobium pentoxide (Nb_2O_5) and their low frequency AC conduction studies are investigated. As the PANI, both in its base form and salt form, has been well studied for its AC conduction and dielectric properties [18–22], the present study will help in understanding the effect of additives on electrical response of PANI. Niobium pentoxide is a white powder, insoluble in acids, but soluble in fused potassium hydrogen sulfate and in carbonate or hydroxide of alkali metals. The melting point of Nb_2O_5

☆ This paper is CEPS communication # 114.
* Corresponding author. Tel.: +91 836 2779983; fax: +91 836 2771275.
E-mail address: aminabhavi@yahoo.com (T.M. Aminabhavi).

0379-6779/$ – see front matter © 2006 Elsevier B.V. All rights reserved.
doi:10.1016/j.synthmet.2006.08.005

is 1520 °C and it has been used extensively as a metal oxide support material in catalysis research due to its high acidity and water-tolerant properties. It has catalytic activity in the selective oxidation in many processes like dehydration of alcohols, partial oxidation of methanol, hydrocarbon conversions, oxidative dehydrogenation, esterification, alkylation, polymerization, methane oxidation, NO decomposition, hydrodesulfurization, photocatalytic decomposition of organic halides, hydrogen absorption, etc. [23]. Apart from the fact that niobates of alkali metals are an important class of ferroelectrics with high dielectric constant, Nb_2O_5 itself finds application in electronic devices. An anodically oxidized Nb_2O_5 thin film has been used as a dielectric material for solid-type electrolytic capacitors, because of its higher dielectric constant and durability than those of the anodically oxidized Al_2O_3 and Ta_2O_5 [24].

As the demand for surface mounted device (SMD) solid electrolyte capacitors has been increasing considerably, Nb_2O_5 with lower raw material price and higher relative permittivity is a good substitute for tantalum in these capacitors [25]. While Nb_2O_5 thick films prepared by conventional methods were used as a resistive-type oxygen sensor [24] and a varistor-type hydrogen sensor [26], anodic oxide films have been tested as a diode-type hydrogen sensor [26]. Niobium oxide with mesoporous structure acts as an electron acceptor and has potential application as electron storage material and fast ion conduction channel for solid electrolyte and battery applications [27,28]. In intercalate and interlayer systems, the host porous oxide framework acts as an electron receptacle for a wide variety of electrochemically active guest species. Its flexible oxidation state behavior allows it to be readily reduced by a wide variety of metallic and organometallic species to lead to a new family of mixed oxidation state intercalates with interesting electronic and even supermagnetic properties [29]. The advantage of this transition metal oxide-based system is that not only the pore size can be varied to allow for intercalation of nanophases of different diameters, but also the propensity for walls to act as electron acceptors can be tuned by doping the walls with metal ions more strongly oxidizing than Nb. This allows control over both the size and electronic structure of the guest phase. Consequently, mesoporous niobium oxide has applications in electronic and magnetic devices [30], biotechnology [31] and nanotechnology [32]. Nb_2O_5, like TiO_2, is a wide band gap semiconductor used in the form of a porous coating of crystalline nanoparticles to develop solar cells [33]. However, in comparison with TiO_2 films, photoelectrochemical properties of Nb_2O_5 films have received little attention regarding their possible use as photovoltaic devices [34]. Similarly, even though polymer composites with TiO_2 have been studied, there are no reports on polymer composites with Nb_2O_5. Hence, in this paper, we present our experimental data on the evaluation of conducting properties of PANI composites containing Nb_2O_5 in order to suggest their applications in electronics and related industries.

2. Experimental

Aniline, ammonium peroxydisulfate (APS), hydrochloric acid (HCl) and Nb_2O_5, all of Analar grade reagents were purchased from s.d. Fine Chemicals, Mumbai, India. Aniline monomer was doubly distilled before use. Deionized water was used throughout the synthetic work. Aniline (0.1 M) was dissolved in 100 mL of HCl (1 M) taken in 500 mL round bottom flask and stirred well. Finely ground Nb_2O_5 powder taken in different (15, 20, 30 or 40) wt.% with respect to aniline concentration was added to the above mixture under vigorous stirring in order to keep Nb_2O_5 powder suspended in solution. The reaction mixture was cooled to 0–5 °C and the pre-cooled solution of ammonium persulfate (0.1 M) was slowly added over a period of 30 min. The reaction was allowed to proceed for 8 h. At the end of the reaction, PANI/Nb_2O_5 composite formed was collected by filtration, washed with distilled water and acetone repeatedly until filtrate was colorless. The collected composite was dried at 100 °C until constant weight was attained. PANI was synthesized in the same manner in the absence of Nb_2O_5.

X-ray diffraction spectra of pristine PANI, Nb_2O_5 and PANI/Nb_2O_5 composites were recorded on a Siemens/D-5000 X-ray diffractometer using Cu Kα radiation (λ = 1.5406 Å). SEM of the pristine PANI and PANI/Nb_2O_5 composites were recorded using the Hitachi S520 scanning electron microscope. TEM of the PANI–Nb_2O_5 composites were recorded on a Technai-12 transmission electron microscope at an acceleration voltage of 100 kV.

The core level XPS spectra of pristine PANI and its composites were recorded using the Shimadzu KRATOS AXIS

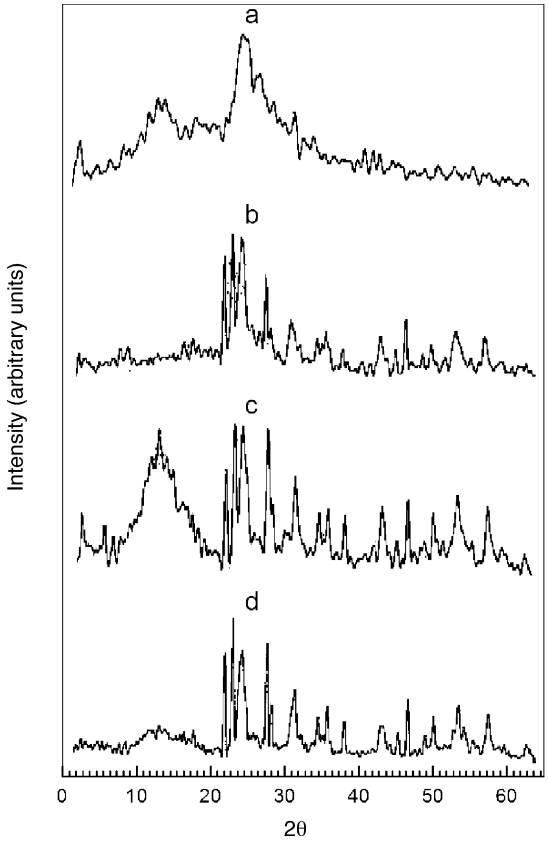

Fig. 1. X-ray diffraction spectra of: (a) pristine PANI, (b) PANI/Nb_2O_5-10%, (c) PANI/Nb_2O_5-30% and (d) Nb_2O_5.

165 X-ray photoelectron spectrometer with Mg Kα source (1253.6 eV).

To measure the AC response, samples were prepared as 1 cm diameter pellets by pressing the powder under a hydraulic pressure of 10,000 psi and then applying conducting silver paste to form the electrodes in contact with the two circular faces. The sample was then held between two nominally spring loaded copper plates and the AC parameters were measured at 300 K using Hioki (Japan) Model 3532-50 programmable LCR meter at the selected frequencies in the range from 100 Hz to 1 MHz.

TGA thermograms of the pristine PANI, Nb_2O_5 and PANI/Nb_2O_5 composites were recorded from 25 to 600 °C at the heating rate of 10 °C/min under nitrogen atmosphere using a Rheometric Scientific (UK) STA Model STA-1500 instrument.

3. Results and discussion

3.1. X-ray diffraction studies

X-ray diffraction patterns of the pristine PANI, Nb_2O_5 and PANI/Nb_2O_5 composites are shown in Fig. 1. The XRD pattern of pristine PANI shows two prominent broad peaks and few smaller peaks riding over a broad hump, indicating that chain ordering is predominantly limited to short range. The broad peaks observed at 24.6° and 26.4° are similar to those observed by others [35]. The XRD pattern for Nb_2O_5 compared well with the JCPDS patterns No. 37-1468 and with the patterns shown in the published literature [36]. XRD patterns of PANI/Nb_2O_5 composites exhibit a predominance of Nb_2O_5 over that of PANI. This implies that the presence of Nb_2O_5 suppresses short-range order in PANI. Further, samples with

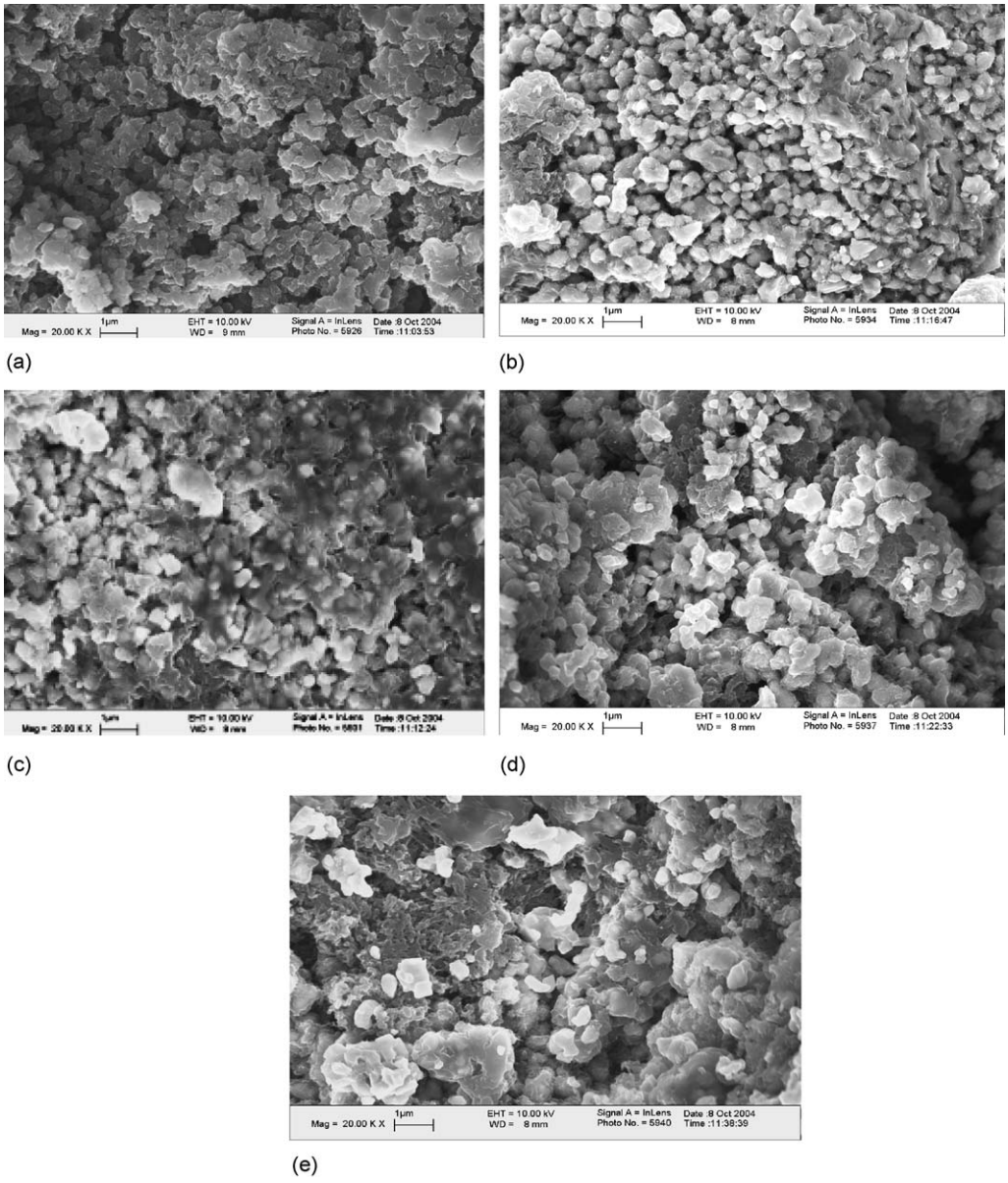

Fig. 2. Scanning electron micrographs of: (a) pristine PANI, (b) PANI/Nb_2O_5-10%, (c) PANI/Nb_2O_5-20%, (d) PANI/Nb_2O_5-30% and (e) PANI/Nb_2O_5-40% composites.

increasing amount of Nb_2O_5 have an increasing disorder. However, the diffraction pattern of Nb_2O_5 in the composites is similar to that of pure Nb_2O_5, indicating that there is no intercalation of PANI into Nb_2O_5 and that PANI deposited on Nb_2O_5 particles has no effect on the crystallization behavior of Nb_2O_5. Applying the Sherrer formula to the most prominent sharp peak at 23°, we obtained the size of the crystallite to be 10 nm. For other peaks that are relatively broader, we got the sizes in the range of 30–40 nm.

3.2. Scanning electron microscopy

SEM micrographs of the pristine PANI and PANI/Nb_2O_5 composites containing different amounts of Nb_2O_5 are displayed in Fig. 2. Pristine PANI (Fig. 2a) shows an aggregated structure, while PANI/Nb_2O_5-10% composite (Fig. 2b) exhibits an aggregated granular morphology. With increasing amount of Nb_2O_5 (20, 30 and 40 wt.%), larger size aggregates are visible, suggesting intermixing of Nb_2O_5 particles with the PANI matrix (see Fig. 2c–e). From the SEM picture of PANI/Nb_2O_5-10% composite, we obtained an average grain size of about 0.5 μm. The size of these grains increases at the higher contents of Nb_2O_5.

3.3. Transmission electron microscopy

TEM picture of PANI/Nb_2O_5-10% composite is shown in Fig. 3a. It is observed that the nono-sized Nb_2O_5 particles are present in PANI matrix as the dispersed individual particles as well as the aggregated small clusters. The size of Nb_2O_5 particles agrees with the size obtained above from the XRD. These particles are covered by PANI layer and hence, TEM presents the morphology of the composite particles as shells with Nb_2O_5 at the core. Such shell structure for composite particles has been reported for other composites in the literature [37,38]. The selected area electron diffraction (SAED) pattern for the composite is shown in Fig. 3b, which indicates a poor crystalline nature of the composite. This supports the inference drawn from the XRD data that the addition of Nb_2O_5 enhances the disorderliness in PANI.

Thus, XRD, SEM and TEM suggest that morphological set up of the composites prepared are made up of mixture of PANI, composite particles with core-shell structure and possibly some uncoated Nb_2O_5. As the wt.% of Nb_2O_5 increases, the extent of composite particles (shells) will also increase (see Fig. 2e).

3.4. X-ray photoelectron spectroscopy

The deconvoluted N (1s) XPS spectrum of PANI/Nb_2O_5-30% composite is displayed in Fig. 4a. The N (1s) curve shows three different kinds of nitrogen at 398.9, 399.5 and 400.8 eV. Intensity of the peak around 399.5 eV is about 50%. However, according to the published reports, the core level N (1s) XPS curve can be deconvoluted into five components at 398.2, 399.39, 400.72, 402.57 and 405.8 eV [39]. The first four peaks are due to amine, imine and the positively charged nitrogen atoms, respectively, whereas the peak observed at 405.8 eV is very weak and is reported to be due to N (1s) shake-up satellite of the ionized nitrogen atoms in PANI chains [40]. The peak around 400.8 eV indicates that some of the imine units are protonated to positively charged nitrogen atoms.

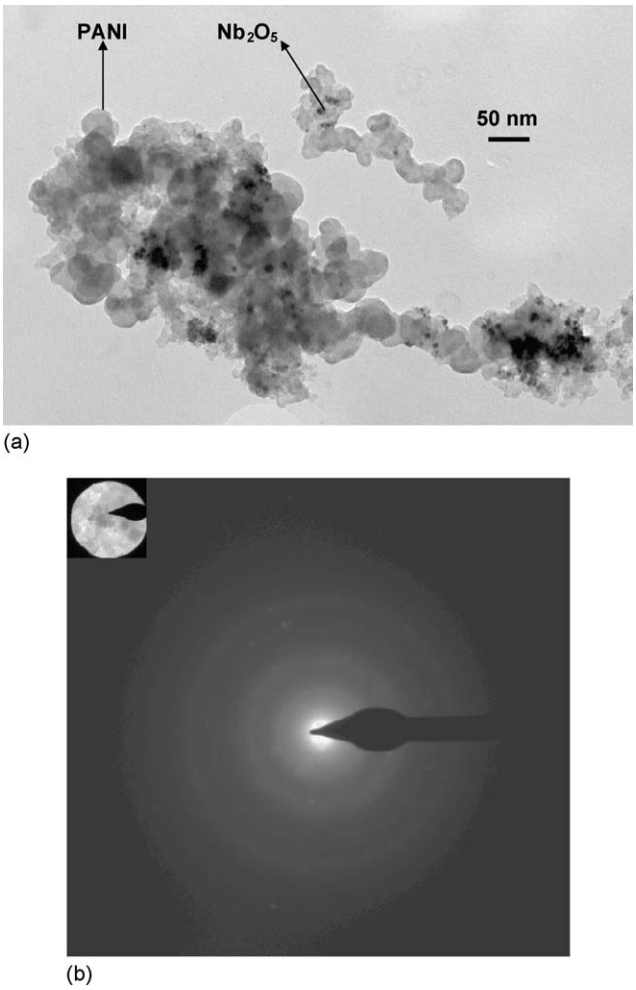

Fig. 3. (a) Transmission electron micrograph of PANI/Nb_2O_5-10% and (b) SAED pattern for PANI/Nb_2O_5-10% composite.

The deconvoluted Cl (2p) XPS spectrum of PANI/Nb_2O_5-20% composite is displayed in Fig. 4b. The Cl (2p) can be split into Cl ($2p_{3/2}$) and Cl ($2p_{1/2}$) with an intensity ratio of 1:2. The Cl ($2p_{3/2}$) is at 197.1 eV, while Cl ($2p_{1/2}$) is observed at 199.0 eV. From the Cl/N ratio, the amount of dopant present in PANI chain is calculated to be 0.25, which matches with that of N^+/N ratio. Since the expected protonation level for the fully doped PANI is generally found to be around 0.5, which suggests that doping of the samples is only moderate. This may be due to leaching of the dopant on account of washing of PANI and the composites by distilled water (rather than 1 M aqueous HCl) during their isolation. In the survey spectrum of the samples (not shown in this paper), we did not observe any characteristic peak corresponding to Nb. Accordingly, the deconvoluted spectrum (Fig. 4b) does not show Nb $3d_{5/2,3/2}$ XPS peaks, which are expected [29] at 206.8 and 209.6 eV. This indicates that Nb_2O_5 is covered by PANI, leading to the formation of shell with Nb_2O_5 at the core.

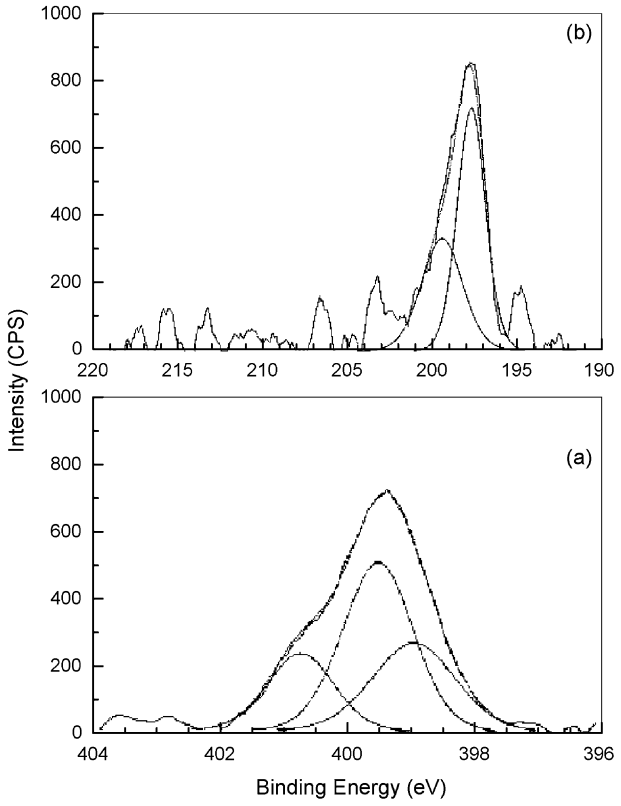

Fig. 4. (a) N (1s) XPS spectra of PANI/Nb_2O_5-30% composite and (b) Cl (2p) XPS spectra of PANI/Nb_2O_5-20% composite.

3.5. Thermogravimetric analysis

Thermal degradation patterns of the pristine PANI and PANI/Nb_2O_5 composites are displayed in Fig. 5. PANI and PANI/Nb_2O_5 composites could undergo a three-stage decomposition pattern. The first stage being weight loss, starting from room temperature to 95 °C corresponds to a loss of water molecules/moisture present in the polymer. The second stage loss from 120 to 320 °C is associated with a loss of dopant ion from the polymer matrix (dedoping). However, the weight loss after 320 °C is due to complete degradation and decomposition of the polymer after the loss of dopant ion [41]. PANI showed a weight loss of 47% up to 600 °C, which decreased after the introduction of Nb_2O_5 into PANI. The PANI/Nb_2O_5-10% matrix showed a weight loss of 33%, which subsequently decreased to 14.5% for PANI/Nb_2O_5-40% composite. However, Nb_2O_5 hardly has shown any weight loss in the scanned region.

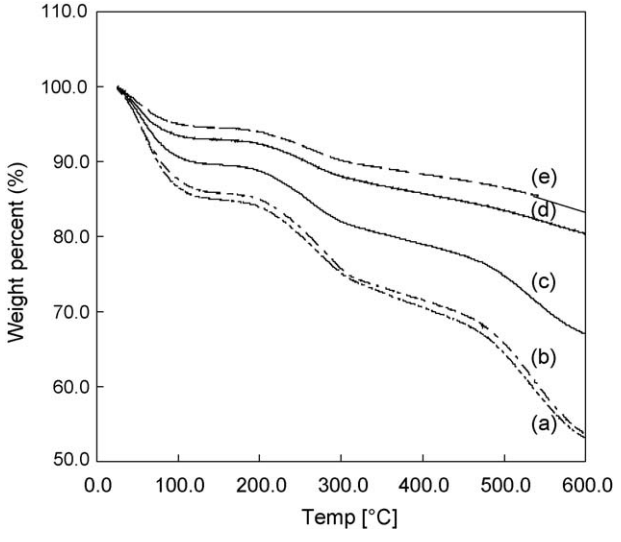

Fig. 5. TGA curves of: (a) PANI, (b) PANI/Nb_2O_5-10%, (c) PANI/Nb_2O_5-20%, (d) PANI/Nb_2O_5-30% and (e) PANI/Nb_2O_5-40% composites.

3.6. AC conduction

Using the values of the equivalent parallel capacitance, C_p, dissipation factor, D, and parallel equivalent resistance, R_p, recorded by the LCR meter at a selected frequency, f, dielectric and conductivity parameters have been calculated using the following equations:

$$\varepsilon' = \frac{C_p}{C_0} \tag{1}$$

$$\varepsilon'' = \frac{\varepsilon'}{\omega C_p R_p} = \varepsilon' D \tag{2}$$

$$\sigma'(\omega) = \omega \varepsilon_0 \varepsilon'' \tag{3}$$

$$\sigma''(\omega) = \omega \varepsilon_0 \varepsilon' \tag{4}$$

where $C_0 = (0.08854A/t)$ pf is the geometrical capacitance of vacuum of the same dimensions as that of the sample; A and t the area and thickness of the sample, respectively; C_p the capacitance measured in pf; $\omega = 2\pi f$ and $D = \tan\delta$, with δ being the phase angle. The ε' and ε'' are, respectively, the real and imaginary parts of the complex dielectric constant $\varepsilon(f) = \varepsilon'(f) - i\varepsilon''(f)$. Similarly, σ' and σ'' are, respectively, the real and imaginary parts of the complex AC conductivity, $\sigma(f) = \sigma'(f) - i\sigma''(f)$. The real part of conductivity, $\sigma'(f)$, shows the features of AC conductivity in disordered materials with two regimes separated by a critical frequency, $f_c = \omega_c/2\pi$. At low frequency, $\sigma'(f)$ is nearly constant, corresponding to DC conductivity, $\sigma(0)$ such that:

$$\sigma'(f) \approx \sigma(0), \quad f \leq f_c \tag{5}$$

At higher frequencies, $\sigma'(\omega)$ increases with frequency and its frequency dependence, according to the hopping model of charge transport in disordered materials, can be approximated by a power law given by [42]:

$$\sigma'(f) \propto f^s, \quad f \geq f_c, \quad \text{with } 0 < s < 1 \tag{6}$$

Notice that f_c is not a well-defined material parameter, which depends upon many factors such as method of synthesis, microstructure formation, composition, etc.

The variation of $\sigma'(f)$ for PANI/Nb_2O_5 composites with frequency is shown in Fig. 6. The $\sigma'(f)$ is almost constant over the low frequency range from 100 Hz to critical frequency, f_c and then, increases with frequency above f_c, in agreement with Eqs. (5) and (6). For pristine PANI (not shown in Fig. 6), measured value of $\sigma'(f = 10\,\text{kHz})$ is of the order of 10^{-4} S/cm; such a low value is attributed to low level of protonation as indicated by

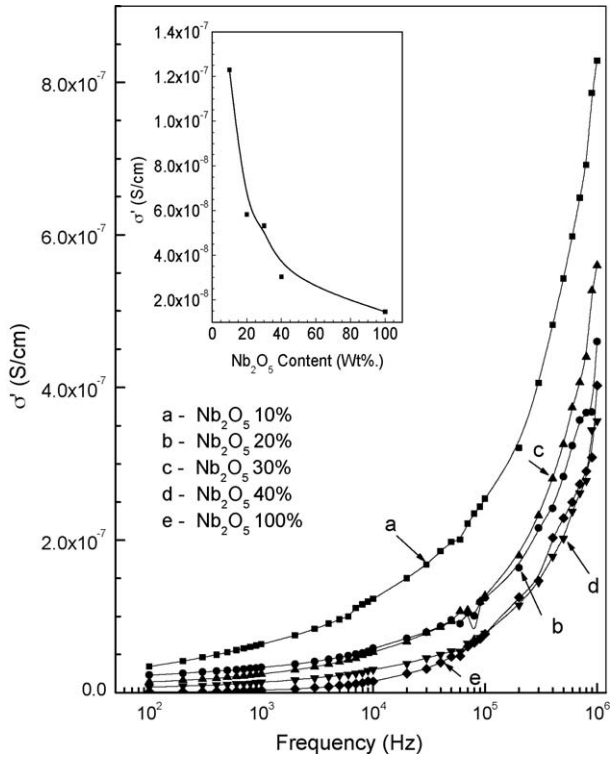

Fig. 6. Frequency dependence of AC conductivity of PANI/Nb_2O_5 composites. *Inset*: Variation of AC conductivity of PANI/Nb_2O_5 composite at 10 kHz with Nb_2O_5 content in the composite.

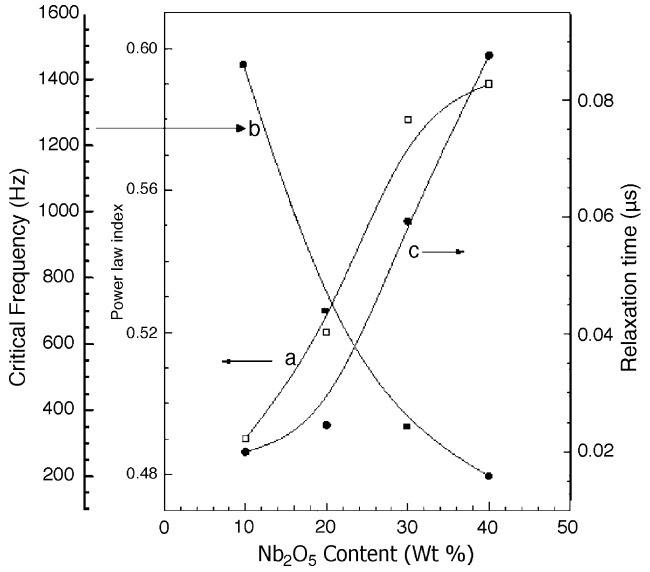

Fig. 7. Variation of: (a) power law index, (b) critical frequency and (c) relaxation time with Nb_2O_5 content in the composite.

XPS and also to low level of crystallinity of the sample as seen in XRD. It is well known that $\sigma'(f)$ depends, apart from frequency f and temperature, on degree of protonation, percent crystallinity, crystalline domain size and order in crystalline and amorphous regions have a relationship with the delocalization length. After taking these factors in to account, we find that our values of $\sigma'(f)$ for PANI compare well with the published data [18–22]. The $\sigma'(f = 10\,\text{kHz})$ of the composites is nearly three orders of magnitude smaller than the pristine PANI, which depends upon the composition.

The dependence of $\sigma'(f)$ on composition is shown in the inset to Fig. 6, which gives the plot of $\sigma'(f = 10\,\text{kHz})$ as a function of wt.% of Nb_2O_5 of the composite. Notice that $\sigma'(f)$ decreases steeply with increasing wt.% of Nb_2O_5 of the composite. This could be due to an increase in the disorderliness of the composite with increasing amount of Nb_2O_5 as also seen from the XRD and TEM data. Nb_2O_5 particles could possibly induce conformational changes in PANI, leading to a reduction in the order and a consequent reduction in the delocalization length, which is reflected with a decrease in conductivity. Further, the observation that conductivity of the composites is higher than that of the pristine Nb_2O_5 and that conductivity decreases with increasing wt.% of Nb_2O_5 will support the morphology of the sample arrived from XRD, SEM and TEM data.

In the domain of validity of power law, the plot of $\log \sigma'(f)$ versus $\log f$ will be a straight line with slope equal to the exponent, s. Using the method of least-squares for linear regression, it is found that over the frequency range above f_c, $\sigma'(f)$ obeys the power law for each of the composition with a power law index, s that slightly varies with frequency and composition. For the best fits, values are as shown in Table 1. We find that s lies between 0.40 ± 0.01 and 0.67 ± 0.01. A temperature independent value of $s = 0.62$ has been reported for doped PANI [20]. However, from Fig. 7, wherein variation of s with composition is displayed, one could see that s increases with increasing wt.% of Nb_2O_5 of the composite. These dependencies are non-linear in nature.

The critical frequency, f_c, may be obtained from the intercept of plots of $\log \sigma'(f)$ and $\log \sigma''(f)$ versus $\log f$. The values so obtained for all the composites are listed in Table 1 and the variation of f_c with composition is also shown in Fig. 7. It is seen that

Table 1
Summary of AC electrical response of PANI/Nb_2O_5 composites

Composition (wt. % of Nb_2O_5)	Real conductivity at 10 kHz, σ' (S/cm)	Power law index, s	Critical frequency, f_c (Hz)	Relaxation time, τ (μs)	Real dielectric constant at 1 kHz, ε'	Dissipation factor at 1 kHz, $\tan\delta$
0	1.43×10^{-4}	0.52	20,000	1.447	176,920	3.319
10	1.23×10^{-7}	0.49	1,443	0.020	100	1.137
20	5.82×10^{-8}	0.52	700	0.024	76	0.776
30	5.31×10^{-8}	0.58	350	0.059	75	0.586
40	3.03×10^{-8}	0.59	200	0.088	58	0.421
100	1.46×10^{-8}	0.67	<100[a]	0.020	50	0.107

[a] In our measurement, the lowest frequency available was 100 Hz.

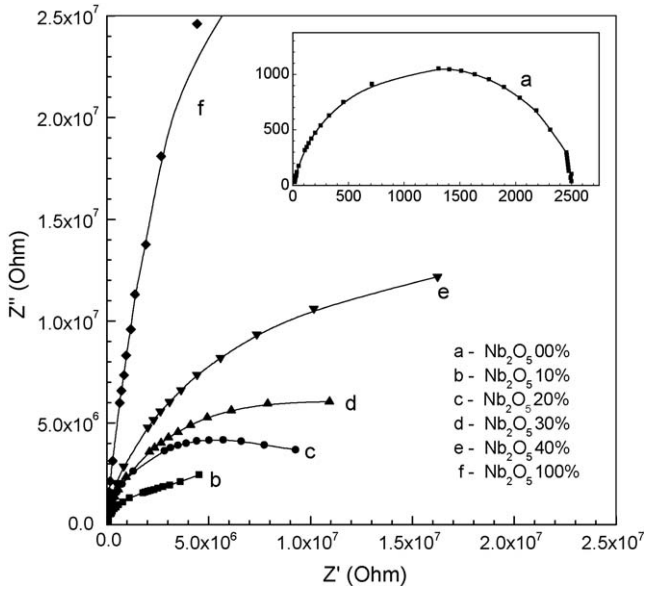

Fig. 8. Complex plane impedance plots for PANI and PANI/Nb_2O_5 composites.

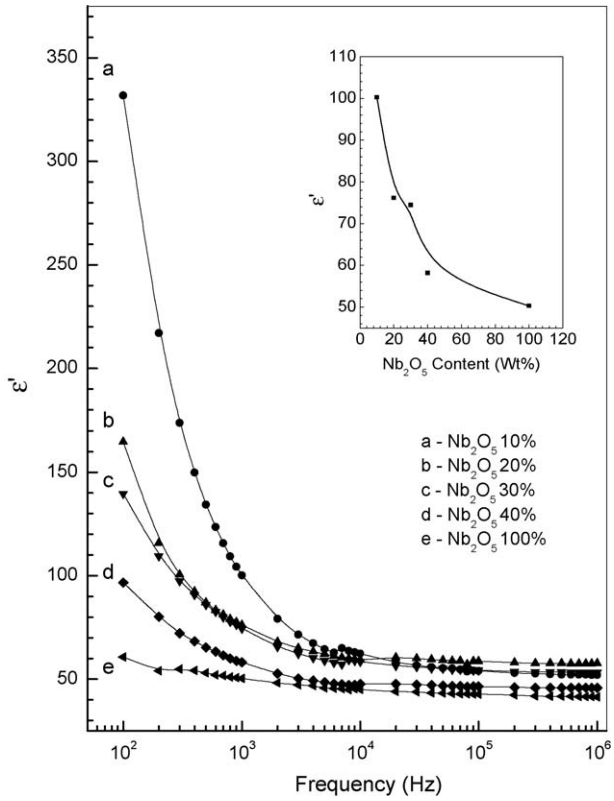

Fig. 9. Frequency dependence of real dielectric constant of PANI/Nb_2O_5 composites. *Inset*: Variation of real dielectric constant of PANI/Nb_2O_5 composite at 1 kHz with Nb_2O_5 content in the composite.

f_c decreases with increasing wt.% of Nb_2O_5, This is expected since f_c is known to decrease with conductivity; notice that in the present composites, conductivity decreases with increasing wt.% of Nb_2O_5. In fact, it is observed that, in the range of 84–300 K, with an increase in conductivity due to increase in doping or temperature, f_c also increases [20].

The complex plane impedance plots for PANI and the composites are displayed in Fig. 8. For pristine PANI, almost semicircular shape of the plot indicates the absence of contact effects and that relaxation nearly follows the Debye model with a single relaxation. The corresponding relaxation time, τ was obtained from this plot using the relation:

$$\tau = \frac{1}{2\pi f_p} \tag{7}$$

where f_p is the frequency corresponding to peak position of the plot, which was obtained by fitting the second order polynomial. A value of 1.447 μs thus obtained agrees with the literature value [43]. However, the presence of a single semicircle for PANI indicates that equivalent circuit for the sample can be represented by a resistance and a capacitor in parallel [43]. According to Dyre, such an electrical circuit is a simple representation of the amorphous semiconductor in which charge transport occurs via electron hopping mechanism [44].

The complex plane impedance plots for all the composites deviate from the semi-circle at higher impedance (lower frequencies), indicating the presence of distribution of relaxation time and conduction losses. However, a careful inspection would reveal that for each of the composites, the first few points in the lower impedance range, corresponding to measurements at high frequencies, fall on a quarter circle, while the remaining points deviate from the circle. Thus, in the high frequency range for each composition, Debye relaxation model may be considered. With increasing Nb_2O_5 content, the frequency region over which this model can be considered shifts towards higher frequency and hence, deviation from this model increases. This may be due to increasing disorder with increasing Nb_2O_5 content of the composite. In order to extract some qualitative information, assuming the validity of Debye model over this quarter circle, peak position of the plot was determined so that f_p and the corresponding relaxation time were obtained for each composition. The values so obtained are shown in Table 1 and the variation of relaxation time with composition is shown in Fig. 7. We see that relaxation time increases with increasing wt.% of Nb_2O_5 of the composite. Since relaxation is related to charge transport by hopping mechanism, an increase in relaxation time indicates the increase in hopping length due to stretching effect of the Nb_2O_5 powder added to PANI, with a consequent reduction in conductivity as seen in Fig. 6. However, the reduction in conductivity with the introduction of Nb_2O_5 need not be considered as the negative result. As mentioned earlier, Nb_2O_5 has the wide ranging applications, which are all well studied. Therefore, its composites with PANI can be tested for some of these applications with the added advantages of flexibility of the polymer. We have some future plans to test the present composites for gas sensor applications.

The observed variation of real part of dielectric constant, $\varepsilon'(f)$, with frequency, f is shown in Fig. 9. For pristine PANI (not shown in Fig. 9), the real dielectric constant has a high value of about 2.9×10^4 at 1 kHz, which decreases with frequency, reaching a value of 1.1×10^4 at 1 MHz. Such large values of real permittivity are not unusual, which are related to effects of electrode polarization and space charge polarization [45]. Like the $\sigma'(f)$,

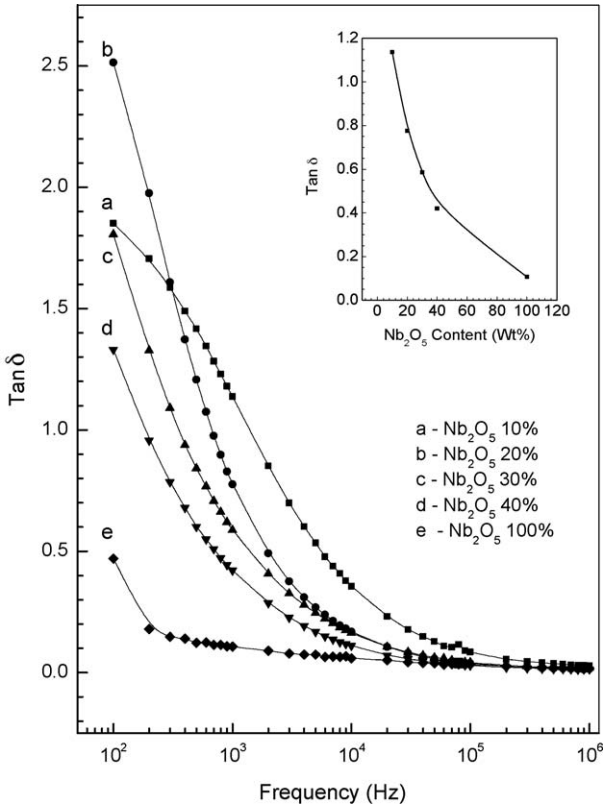

Fig. 10. Frequency dependence of dissipation factor of PANI/Nb_2O_5 composites. *Inset*: Variation of dissipation factor of PANI/Nb_2O_5 composite at 1 kHz with Nb_2O_5 content of the composite.

$\varepsilon'(f)$ also increases with protonation, temperature and delocalization length [18,20–22]. Notice that $\varepsilon'(f)$ of the composites is two orders of magnitude smaller than that of the pristine PANI and it depends upon the composition. Dependence of $\varepsilon'(f)$ on composition is shown in the inset to Fig. 9, which gives a plot of $\varepsilon'(f = 1\,\text{kHz})$ as a function of wt.% of Nb_2O_5 in the composite. It is seen that ε' decreases steeply with increasing wt.% of Nb_2O_5. From the conductivity data (Fig. 6) and the dielectric data (Fig. 9), it is instructive to note that, in the low frequency region, both the $\sigma'(f)$, which is considered as DC conductivity and $\varepsilon'(f)$ are nearly two orders of magnitude smaller in composites and decrease further with increasing wt.% of Nb_2O_5 in the composites. Thus, a reduction in $\varepsilon'(f)$ along with $\sigma'(f)$ supports the above expressed view that in the low frequency region, conduction relaxation contributes to the high value of $\varepsilon'(f)$.

The dissipation factor, $\tan\delta$, recorded as a function of frequency for PANI/Nb_2O_5 composites is shown in Fig. 10. The loss tangent for PANI (not shown in Fig. 10) has a rather high value of 4.66 at 100 Hz, which decreases with increasing frequency, reaching a value of 0.23 at 1 MHz. Similar value that increases with protonation has been reported earlier [20]. Loss tangent in composites is almost half of that observed for the pristine PANI, which shows a similar behavior with frequency. However, none of the loss tangent curves show a peak in the measured frequency range of 100 Hz–1 MHz. As noted earlier, high loss at low frequency in all the composites may be attributed to DC conduction losses. The loss tangent at 1 kHz taken from these graphs is shown in Table 1 and is plotted as a function of composition in the inset of Fig. 10. We see that dielectric loss also decreases with increase in wt.% of Nb_2O_5. This is expected because conductivity decreases with increase in wt.% of Nb_2O_5.

It is important to recognize that Table 1 and Fig. 7 not only summarize the present data on the effect of composition on AC electrical response of the composite as measured through different parameters, but also they help to find the interdependence of these parameters. We see that in the low frequency region, conductivity, real dielectric constant and dissipation factor decrease with increasing content of Nb_2O_5, indicating the role of conduction charges in dielectric response. Similarly, the decrease in critical frequency is related to a decrease in conductivity. In addition, we may point out that variations in the parameters listed in Table 1 with increasing content of the composite are similar to the reported variations of these parameters with a decrease in temperature. If this observation is seen with the observation [19] that the effect of temperature in the range of 84–300 K is similar to that of doping, since both f_c and DC conductivity increase with temperature, as they do with doping, we may deduce an interesting inference that the effect of increasing Nb_2O_5 content in the composite is similar to that of decreasing doping level.

4. Conclusions

A great deal of research has been made on conducting polymers since the pioneering work of MacDiarmid, Heeger and Shirakawa and since then, their applications in electronics, optoelectronics and energy storage devices have been increasing exponentially. In the present research, conducting polyaniline/niobium pentoxide nanocomposites with moderate protonation have been synthesized by in situ polymerization of aniline in the presence of Nb_2O_5. XRD and SAED patterns show a decrease in crystallinity with increasing content of Nb_2O_5. AC conductivity obeys the power law well above the critical frequency for each composite. The decrease in AC conductivity with an increase in wt.% of Nb_2O_5 is attributed to conformational changes in PANI and increased disorder. In view of the wide ranging applications of Nb_2O_5 as catalyst, solid electrolyte for battery and capacitor, tunable mesoporous host for intercalates with exciting properties, solar cell coating, gas sensing, absorption, etc., its composites with PANI can be tested for some of these applications with the added advantages of flexibility. While PANI shows nearly a Debye-type single relaxation, the composites show a distribution of relaxation time. Interestingly, the variation in electrical response with an increase in the content of Nb_2O_5 of the composites is similar to the reported variations with a decrease in temperature or doping level.

Acknowledgements

The authors (Professor T.M. Aminabhavi and Dr. M. Sairam) appreciate the financial support from University Grants Commission (UGC), New Delhi, India (F1-41/2001/CPP-II), to establish Center of Excellence in Polymer Science (CEPS). This paper is originated from the MoU between CEPS and The University of Texas, Dallas, USA. It is also a collaborative effort

between CEPS and Department of Physics, Gulbarga University, Gulbarga.

References

[1] C.G. Wu, D.C. Degroot, H.O. Marcy, J.L. Schindler, C.R. Kannewurf, Y.J. Liu, W. Hirpo, M.G. Kanatzidis, Chem. Mater. 8 (1996) 1992.
[2] T.A. Kerr, H. Wu, L.F. Nazar, Chem. Mater. 8 (1996) 2005.
[3] E.R. Hitzky, P. Aranda, B. Casal, J.C. Galvan, Adv. Mater. 7 (1995) 180.
[4] W.J. Bae, K.H. Kim, W.H. Jo, Y.H. Park, Macromolecules 37 (2004) 9850.
[5] A.G. MacDiarmid, J.C. Chiang, M. Halpern, W.S. Huang, S.L. Mu, N.L.D. Somasiri, W. Wu, S.I. Yaniger, Mol. Cryst. Liq. Cryst. 121 (1985) 173.
[6] A.G. MacDiamid, J.C. Chiang, A.F. Richter, A.J. Epstein, Synth. Met. 18 (1987) 285.
[7] P. Somani, B.B. Kale, D.P. Amalnerkar, Synth. Met. 106 (1999) 53.
[8] F. Fusalba, D.J. Belangar, Mater. Res. 14 (1999) 1805.
[9] M.L. Gautu, P.J.G. Romero, Solid State Chem. 147 (1999) 601.
[10] I. Krivka, J. Prokes, E. Tobolkova, J. Stejskal, J. Mater. Chem. 10 (1999) 2425.
[11] W. Jia, E. Segal, D. Kornemandel, Y. Lamhot, M. Norkis, A. Siegmann, Synth. Met. 128 (2002) 115.
[12] S.J. Su, N. Kuramoto, Synth. Met. 114 (2000) 147.
[13] S. Wang, Z. Tan, Y. Li, L. Sun, T. Zhang, Thermochim. Acta 441 (2006) 191.
[14] J.W. Kim, S.G. Kim, H.J. Choi, M.S. Jhon, Macromol. Rapid Commun. 20 (1999) 450.
[15] C. Wang, Y.H. Zang, J.B. Gao, W.J. Zang, Y.F. Lu, Y.B. Bai, T.J. Li, L.J. Li, Y. Wei, Chem. J. Chin. Univ. 20 (1999) 1491.
[16] B.Z. Tang, Y. Geng, J.W.Y. Lam, B. Li, X. Jing, X. Wang, F. Wang, A.B. Pakhomov, X.X. Zhang, Chem. Mater. 11 (1999) 1581.
[17] B.Z. Tang, CHEMTECH 29 (1999) 7.
[18] F. Zuo, M. Angelopoules, A.G. MacDiarmid, A.J. Epstein, Phys. Rev. B 39 (1989) 3570.
[19] R.F. Bianchi, G.F. Leal Ferreira, C.M. Lepienski, R.M. Faria, J. Chem. Phys. 110 (1999) 4602.
[20] H.H.S. Javadi, K.R. Cromack, A.G. MacDiarmid, A.J. Epstein, Phys. Rev. B 39 (1989) 3579.
[21] N.J. Pinto, P.D. Shah, P.K. Kahol, B.J. McCormic, Solid State Commun. 97 (1996) 1029.
[22] J. Joo, Z. Oblakowaski, G. Du, J.P. Pouget, E.J. Oh, J.M. Wiesinger, Y. Min, A.G. MacDiarmid, Phys. Rev. B 49 (1994) 2977.
[23] V.S. Braga, J.A. Dias, S.C.L. Dias, J.L. de Macedo, Chem. Mater. 17 (2005) 690.
[24] T. Hyodo, J. Ohoka, Y. Shimizu, M. Egashira, Sens. Actuators B: Chem. 117 (2006) 359–366.
[25] V. Fischer, H. Störmer, D. Gerthsen, M. Stenzel, H. Zillgen, E. Ivers-Tiffée, Proceedings of the 7th International Conference on Properties & Applications of Dielectric Materials (ICPADM 2003), Nagoya, Japan, June 1–5, 2003, S20-2.
[26] T. Hyodo, E. Kanazawa, Y. Takao, Y. Shimizu, M. Egashira, Electrochemistry 68 (2000) 24.
[27] M. Vettraino, M. Trudeau, D.M. Antonelli, Adv. Mater. 12 (2000) 337.
[28] D.R. MacFarlane, J. Huang, M. Forsyth, Nature 402 (1999) 792.
[29] X. He, M. Trudeau, D. Antonelli, Adv. Mater. 14 (2000) 12.
[30] M. Vettraino, X. He, M. Trudeau, D.M. Antonelli, J. Mater. Chem. 11 (2001) 1755–1759.
[31] L. Washmon-Kriel, V.L. Jimenez, K.J. Balkus Jr., J. Mol. Catal. B: Enzym. 10 (2000) 453.
[32] B. Ye, M.L. Trudeau, D. Antonelli, Adv. Mater. 13 (2001) 29.
[33] A. Michel Aegerter, Solar Energy Mater. Solar Cells 68 (2001) 401.
[34] L. Hu, W. Marcus, M. Gratzal, Z. Jiang, J. Sol–Gel Sci. Technol. 5 (1995) 219.
[35] H. Ali Gemeay, A. Ikhalas Mansour, G. Rehab El-Sharkawy, B. Ahmed Zaki, Eur. Polym. J. 41 (2005) 2575.
[36] I.C.M.S. Santos, L.H. Loureiro, M.F.P. Silva, M.V. Ana, Polyhedron 21 (2002) 2009.
[37] A. Dey, S. De, A. De, S.K. De, Nanotechnology 15 (2004) 1277.
[38] S.S. Ray, M. Biswas, Mater. Res. Bull. 34 (1999) 1187.
[39] X.R. Zeng, T.M. Ko, Polymer 39 (1998) 1187.
[40] B. Sjogren, W.R. Salaneck, S. Stafstorm, J. Chem. Phys. 97 (1992) 3674.
[41] S.F. Patil, A.G. Bedekar, C. Agashe, Mater. Lett. 14 (1992) 307.
[42] J. Bisquert, G. Garcia-Belmonte, Russ. J. Electrochem. 40 (2004) 352.
[43] D. Hui, R. Alexandrescu, M. Chipara, I. Morjan, Gh. Aldica, M.D. Chipara, K.T. Lau, J. Optoelectron. Adv. Mater. 6 (2004) 817.
[44] J.C. Dyre, J. Appl. Phys. 64 (1988) 2456.
[45] H.M. Kim, C.Y. Lee, J. Joo, Korean Phys. Soc. 36 (2000) 371.